Aging behavior of a 1.5 mol% yttria doped zirconia exhibiting optimized toughness and strength

M. Imariouane, M. Saâdaoui, Sandrine Cardinal, Helen Reveron, Jérôme Chevalier

▶ **To cite this version:**

M. Imariouane, M. Saâdaoui, Sandrine Cardinal, Helen Reveron, Jérôme Chevalier. Aging behavior of a 1.5 mol% yttria doped zirconia exhibiting optimized toughness and strength. Journal of the European Ceramic Society, 2024, 44 (2), pp.1053-1060. 10.1016/j.jeurceramsoc.2023.09.041 . hal-04297460

HAL Id: hal-04297460
https://hal.science/hal-04297460

Submitted on 21 Nov 2023

HAL is a multi-disciplinary open access archive for the deposit and dissemination of scientific research documents, whether they are published or not. The documents may come from teaching and research institutions in France or abroad, or from public or private research centers.

L'archive ouverte pluridisciplinaire **HAL**, est destinée au dépôt et à la diffusion de documents scientifiques de niveau recherche, publiés ou non, émanant des établissements d'enseignement et de recherche français ou étrangers, des laboratoires publics ou privés.

Aging behavior of a 1.5 mol.% yttria doped zirconia exhibiting optimized toughness and strength

M. Imariouane[1], M. Saâdaoui[1], S. Cardinal[2], H. Reveron[2], J. Chevalier[2]

[1]Université Mohammed V de Rabat, EMI, Avenue Ibn Sina, 10000 Rabat, Morocco

[2]Université de Lyon, INSA de Lyon, Université Claude Bernard Lyon 1, CNRS, MATEIS, UMR5510, Villeurbanne, France

Abstract

The aging behavior of a 1.5Y-TZP with 0.25%wt of alumina exhibiting high mechanical properties was investigated in both water vapor and in air with in situ XRD analysis. The results showed that the material exhibited a high resistance to aging in water vapor at 134°C compared to 3Y-TZP, which is explained by the addition of alumina and a lower sintering temperature. The aging kinetics were fitted by the Mehl–Avrami–Johnson law, three stages were identified corresponding to predominance of nucleation mechanism for temperatures below 180°C and above 340°C and to growth mechanism for intermediate temperatures. It was shown that for the temperature range investigated in water vapor and air, the mechanism was independent on the environment. A strong influence of the cooling rate on the tetragonal to monoclinic phase transformation was observed and discussed using a time–temperature-transformation diagram derived from the aging results in air.

Keywords: 1.5Y-TZP, low temperature degradation, aging kinetics, activation energy, time-temperature-transformation curves.

1. Introduction

Yttria-doped Tetragonal Zirconia Polycrystalline (Y-TZP) ceramics have become a popular choice in engineering and in particular biomedical applications due to their biocompatibility, and their mechanical properties including high strength and high toughness. This can be attributed to the retention of the high temperature tetragonal phase of zirconia at room temperature by addition of yttria (Y_2O_3), typically in the range of 2 to 3.5 mol%, leading to the transformation toughening mechanism due to stress-induced martensitic tetragonal to monoclinic (t-m) phase transformation [1-3].

One point of vigilance with Y-TZPs is their sensitivity to a spontaneous (i.e. without the need of applied stress) and progressive t-m phase transformation in a humid environment, within a temperature range typically from room temperature to 400°C [4-9]. This phenomenon known

as aging or Low Temperature Degradation (LTD), may have negative effects as surface roughening, enhanced wear rates or loss of mechanical properties [6,10-13]. Most of the experimental work on LTD in Y-TZP was focused on accelerated aging of 3Y-TZP (i.e., 3 mol.% yttria doped zirconia) in autoclave conditions with water vapor, as well documented in numerous review articles such as [3,7,13,14]. Indeed, for biomedical applications, aging at 134 °C under 2 bars pressure for 5 h corresponds roughly to 20 years in vivo [15].

The prevailing explanation for the mechanism of LTD revolves around the increase of internal stresses caused by the intrusion of water molecules into the lattice structure [11,16,17]. This process triggers the t-m phase transformation, setting off a sequence of events where the transformation initially takes place within individual grains and progressively extends to the surface of the sample then continues inward, via a nucleation-and-growth (N-G) mechanism [11,18-21], leading to the development of micro-cracks [22,23]. Various strategies have been employed to avoid or reduce the effect of aging in Y-TZP, among which, decreasing the grain size [24-27], and increasing the yttria content [28-32], both resulting in less t-m phase transformability, which may have a negative impact on mechanical properties. Resistance to LTD can also be improved by increasing Y^{3+} ion concentration in the tetragonal phase by decreasing the sintering temperature [8,33], or by using additional dopants such as silica glassy phase [34,35], CeO_2 [36] or alumina [32,37,38].

For Y-TZP ceramics, LTD kinetics has been often fitted by the Mehl-Avrami-Johnson (MAJ) equation [39-43]:

$$V_m = 1\text{-}exp\ (\text{-}(b.t)^n) \qquad (1)$$

where V_m is the volume fraction of the monoclinic phase, t is the time, and b and n are constants depending on the temperature.

It has been shown [19] that the exponent n, typically ranged from 0.3 to 4, is related to the ratio between nucleation and growth rates. Specifically, when n takes low values, typically < 1, nucleation is the dominant mechanism, whereas high values of n indicate that growth plays a more significant role. As indicated in Table 1, the majority of studies reported low values for the parameter n for temperatures below 200°C, which suggests that the nucleation process is dominant at this temperature range.

Combining the data obtained at different temperatures, the transformation kinetics form ‘‘C’’-shaped curves on a time–temperature-transformation (TTT) plot [38,41,44-48]. At temperatures well below the nose, the kinetics follow an Arrhenius dependence:

$$b = b_0 . exp\left(\frac{-Q}{RT}\right) \quad (2)$$

where the term b_0 is a constant (pre-exponential factor), R is the gas constant, T is the temperature and Q is the activation energy for which the reported values are close to 100 kJ/mol (tab1), which correspond to the activation energy for oxygen vacancy diffusion [3].

Besides hydrothermal accelerated aging, it is also important to characterize LTD in air as it can occur during cooling after sintering or heat treatments, or simply during the use for engineering applications other than the biomedical field. However, only a few studies were dedicated to the aging of Y-TZP ceramics in air and they have almost been performed separately, without a direct comparison with the results in the presence of water vapor. Moreover, the values of the kinetics exponent n in MAJ law (eq.2) are lacking for temperatures above 200°C and Y_2O_3 content less than 3% mol. (tab 1).

In the present work, the aging behavior of a 1.5Y-TZP zirconia with 0.25 wt % Al_2O_3 developed by Tosoh (Japan) under the tradename 'Zgaia 1.5Y-HT' [49] is deeply investigated both in water vapor and in air, within the temperature range from 100 to 400°C. In a previous work [50], it has been shown that this material exhibits high level of both strength (1 GPa) and toughness (8.5 MPa$\sqrt{m}$), near the optimum between a brittle (crack propagation followed by transformation-toughening) and a ductile (transformation induced plasticity, before crack propagation) behavior [51]. It could thus be used in structural applications requiring high toughness and thus flaw tolerance. The question of metastability and thus aging might be raised for such low yttria content and high transformability under stress. However, the material was designed to be sintered at low temperature (e.g., full density already reached at 1350°C for 2 h), thanks in part to the addition of 0.25 mass% Al_2O_3, leading to a homogeneous distribution of yttria in the grains and no yttria depletion to grain boundaries [52]. It was thus one objective of the present study, beside the comparison of aging mechanisms in water and air, to assess the stability of this material during isothermal treatments and upon cooling.

Table 1: MAJ parameter, *n*, and activation energy, *Q*, for Y-TZP ceramics aged in air or in water vapor. T_A is the temperature of aging.

Medium	Y_2O_3 (% mol)	Al_2O_3 (% wt)	Grain size (nm)	T_A (°C)	*n*	*Q* (kJ/mol)	Reference
Water vapor	2	0	510	140	~1	-	[53]
	2.5	0-27.5*	450-600	134	~1	-	[54]
	3	0	180	134	0.75	-	[55]
		0	210	134	-	98	[32]
		0	< 320	134	1.04	-	[56]
		0	330	100-137	0.94 -1.29	89	[57]
		0	370	134	1.15	-	[58]
		0	450	140	~1	-	[53]
		0	500	70 - 130	3.6	106	[39]
		0	540	130 - 140	2	88.9	[42]
		0	350-700	134	0.97	-	[59]
		0	-	134	1	-	[60]
		0	-	120 - 140	1.5	96	[61]
		0	-	120 - 140	0.6	104	[61]
		0	-	140	1.7	-	[62]
		0.05	304	134	1.29	-	[63]
		0.25	225	134	-	109	[32]
		0.25	305	134	1.06	-	[63]
		0.25	-	100-140	-	93	[64]
		0.25	500	134	0.7	-	[65]
		0.43	270- 800	140	1.5	-	[66]
		2	217	134	-	107	[32]
		5	214	134	-	105	[32]
		1-24**	-	130	0.8 - 1.4	-	[67]
		-	320-770	85 - 140	0.92	115.3	[43]
		-	260-690	134	0.47- 1.54	-	[68]
	4	0	550	140	~ 2	-	[53]
Air	3	0	470-770	130 - 220	-	81	[69]
		0	550- 850	100 - 220	-	83	[70]
		0	-	127, 200	1.4	~100	[38]
		0.02	-	80	0.7	-	[71]

* in vol.%.

** in mol %

2. Material and Methods

The material used in this study was a 1.5 mol% Yttria stabilized zirconia (1.5Y-TZP), provided by Tosoh (Japan) in the form of sintered and polished samples (with diamond pastes down to 1 µm). Addition of 0.25 wt.% Al_2O_3 allowed for its sintering at relatively low temperature (1350°C for 2 hours) compared to conventional Y-TZP. In a previous study [50], it was shown that the average grain size of the material, evaluated by the linear-intercept method, was 440 nm and that it exhibited a strong transformability under stress, leading to a high toughness (8.5 MPa$\sqrt{m}$) while keeping a bending strength of around 1 GPa.

To investigate the susceptibility of the material to LTD, hydrothermal and dry aging tests were carried out on polished samples, respectively in a humid environment and in air. The progress of aging was monitored by the variation of the volume fraction of the monoclinic content, determined as indicated in [72,73], from X-Ray Diffraction (XRD) patterns recorded on the polished surfaces within the 2θ angular range of 27° to 32°, using a D8 Advanced Bruker AXS diffractometer (Billerica, USA, CuKα1). Hydrothermal aging tests were carried out using a stainless-steel autoclave where the samples were exposed to water vapor under a pressure of 2 bars, for different durations, at temperatures between 100 and 140°C. Dry isothermal transformation was investigated at various temperatures between 120 and 400°C, with in situ high temperature X-ray diffraction (HTXRD). Intensity data were collected by a linear detector (LynxEye) in PSD fixed scan mode. High temperature experiments were performed in air atmosphere using an Anton Paar HTK 1200 furnace chamber. The samples were first heated from ambient temperature to the desired temperature, at a heating rate of 0.5°C/s. After a holding time of 5 seconds, XRD patterns were recorded with a frequency varying from 3 minutes to 1 hour, depending on the rate of transformation that varied with the temperature.

The effect of the cooling rate on the t-m transformation after annealing was investigated using HTXRD. Some samples were heated with a heating rate of 0.5°C/s up to a temperature of 600°C, where they were held for 20 minutes, then they were cooled down to room temperature at cooling rates ranging from 1 to 12°C/min. XRD patterns were recorded during cooling at different frequencies depending on the cooling rate. The reverse transformation from monoclinic to tetragonal phase during heating was also investigated using HTXRD. Samples were subjected to heating from room temperature up to 1200°C at a rate of 5°C per minute. During the heating process, XRD patterns were recorded at intervals of 4 minutes.

Optical microscopy (ZEISS Axiophot) was used with Nomarski contrast to observe the evolution of the surface topography of the samples after different heat treatments or aging tests.

3. Results

3.1. Hydrothermal aging

Figure 1 shows the variation over time of the monoclinic content, V_m, during hydrothermal aging at temperatures ranging from 100 to 140°C. The monoclinic phase content increases with time, with increasing transformation rate with rising temperature. After 30 hours in autoclave, V_m is less than 20% at 100°C and reached respectively 39%, and 48% at 134, and 140°C.

3.2. Dry aging

Figure 2 shows an example of in-situ HTXRD patterns during aging in air at 250°C. At this temperature, the monoclinic content increases rapidly, from 3% to 85% within less than 8.10^3 seconds (i.e., roughly 2 hours). Figure 3 illustrates the variation with aging time in air of the monoclinic content at various temperatures ranging from 120 to 360°C. Transformation rate increases first from 120°C to 275°C, for which the kinetics is the most rapid, and then decreases again. At that 'nose' temperature, the monoclinic content reached 80% (saturation) after only half an hour. An isothermal test was also carried out at 400°C, but no transformation occurred at this temperature after more than 50 hours (not presented in the figure, since showing a constant value of V_m). This temperature can thus be considered as an approximate value of the start temperature for the martensitic t-m transformation, M_s.

3.3. Effect of the cooling rate on the t-m transformation

Figure 4 presents the variation of the volume fraction of the monoclinic phase with temperature during cooling from 600°C at different cooling rates. The arrow in the figure shows the direction of temperature variation. No transformation was observed for a sample cooled at 12°C/min. As the cooling rate was decreased, t-m phase transformation occurred earlier and earlier, with increasing transformation rate. For a cooling rate of 9°C/min, the transformation started around 350°C then continued slightly and saturated at a temperature about 200°C, with a final monoclinic content of 15%. At cooling rates of 4.5°C and 1°C/min, the transformation started respectively at 380°C and 400°C and the monoclinic content rose rapidly to final rates respectively of 84% and 90%. These results are in line with a martensitic start transformation temperature, M_s, of about 400°C.

3.4. Reverse monoclinic to tetragonal phase transformation

Figure 5 shows the monoclinic content as a function of temperature during heating from room temperature up to 1200°C, at a rate of 5°C/min, of a sample with an initial monoclinic content of 87% (obtained after prior annealing at 1200°C and cooling at a rate of 5°C/min). The arrow in the figure indicates the direction of temperature variation. No transformation was observed before the temperature of 380°C at which the reverse m-t transformation was initiated and then continued slightly until the temperature of 580°C, at which an abrupt loss of the monoclinic content to 4% was observed. This temperature can thus be considered as the austenite start temperature (A_s) and agrees well with a roughly 200°C difference between As and Ms in zirconia systems [74]. The fact that the monoclinic content already slightly but significantly varies before A_s and even starting at 200C° would require further exploration, but seems in line with the saturation level of monoclinic content during the aging experiments presented in figure 3, with a maximum value of V_m of about 90% at temperatures below 200°C and of roughly 70% at 350°C.

4. Discussion

4.1. LTD resistance and Kinetics

XRD results presented in Figure 1 reveal that during accelerated hydrothermal aging at 134°C (corresponding to the ISO 13356 standard procedure) the variation of the monoclinic fraction reached 14% after 5 hours of aging. In contrast, under the same conditions, standard 3Y-TZP without alumina addition exhibited a variation of the monoclinic fraction of 27% [50]. These findings indicate that the studied 1.5Y-TZP exhibits superior resistance to LTD compared to conventional 3Y-TZP and follows requirements of ISO 13356 standards for biomedical applications. This can be attributed to the addition of alumina that leads to the segregation of Al^{3+} cations at the grain boundaries, which contributes to retarding the progression of LTD [32,75]. Another factor contributing to the resistance to LTD of the present material is its relatively low sintering temperature (1350°C), which helps prevent phase partitioning, yttria depletion towards cubic grains and thus leads to a homogeneous distribution of yttria in the grains [3,52]. Yttria depletion occurs for materials sintered at high temperatures and consists of the formation of yttrium-rich cubic and yttrium-poor tetragonal phases. As depleted tetragonal grains are less stable to transformation, they act as preferential nucleation sites for LTD [8,76]. The low sintering temperature of this material, and of Y-TZP in general, is thus a key for improved aging resistance.

The transformation curves (Fig. 1 and 3) were fitted by the MAJ law (eq. (2)), linear plots of which (ln (ln (1/(1 – V_m)) versus ln t) are presented in figures 6 and 7 respectively for aging in water vapor and air. It can be seen that for both environments, a linear relationship is observed at all temperatures, which suggests nucleation and growth kinetics. The values of the exponent n, derived from the slope of the straight lines are reported as a function of temperature in Figure 8, in which three stages could be distinguished. The first stage corresponds to temperatures below 180 °C, for which n values are about 0.6, independently of temperature and environment. This is in agreement with the majority of the values reported for this range of temperature (Tab. 1) and indicates that there is a high nucleation rate with the growth rate kinetically limited by the growth velocity of the interface between the tetragonal and monoclinic phases [3,19,44,71]. At around 180°C, n experienced an abrupt increase then stabilized between 3 and 4, until 340°C (second stage). This can be attributed to a change of transformation kinetics within this temperature range, where three-dimensional growth process became dominant, with the rate of nucleation being limited by the driving force for the nucleation of the monoclinic phase and the growth rate being increased by temperature [3,19]. At the third stage corresponding to temperatures above 340°C, the exponent n goes back to small values (~ 0.6), which indicates that the nucleation process becomes again dominant. Overall, at temperatures above 340°C, the aging kinetics were slow since the temperature is approaching M_s.

The three stages were confirmed by optical observations, as shown in Figure 9 where examples of optical micrographs obtained under Nomarski contrast of samples aged at various temperatures are presented. At 134°C and for all temperatures within the first stage, only nucleation sites, examples of which are indicated by arrows in the figure, were observed. At 250°C and 275°C (corresponding to the second stage), large domains generated through the growth process were observed, with increasing size as the temperature was increased. After aging at 360°C which is within to third stage, the shape of the surface is similar to that observed at low temperatures, with only nucleation sites.

The apparent activation energy, Q, provides insight into the mechanism of the t-m phase transformation during aging. To determine this parameter, the kinetic parameter, b (eq. (2)), was deduced by MAJ fitting (Fig. 6 and 7) and ln(b) was plotted versus 1/T. The results presented in figure 10 show a linear relationship and Q was estimated to be 90 kJ/mol independently on the environment, with a correlation coefficient of 98%. This value aligns with previous findings shown in Table 1, and corresponds closely to the activation energy for oxygen vacancies diffusion in Y-TZP ceramics (~ 100 kJ/mol) [3].

The similitude of the exponent n and the apparent activation energy, Q, in air and in water vapor (within the studied temperature range for the latter case, i.e. 120 to 140°C) suggests that the moisture content does not affect significantly the kinetics of aging and the activation energy in this range of humidity content and temperature. Thus, the humidity in the air is sufficient to activate isothermal transformation. As no information is available for n values at high temperatures in humid environment, further work is underway to investigate the effect of humidity on the second and the third stages observed in air.

4.2. TTT curves and consequences

A TTT diagram has been derived from aging data in air (Fig. 3) and the results are presented in Figure 11, which indicates the times corresponding to monoclinic contents of 15%, 50%, and 75%. The start temperature for the t-m transformation, M_s, is also indicated in the figure. Distinctive C-shaped curves can be seen with a "nose" at a temperature of 275°C, corresponding to the fastest transformation. This shape, also observed by others authors for Y-TZP materials [38,41,44-48,77], can be explained by the competition between the driving forces for nucleation (difference between actual temperature and M_s) and growth mechanisms (temperature itself) [41]. At temperatures below the nose, the nucleation rate is significantly high, and the growth rate is constrained by the kinetics of the interface between the tetragonal and the monoclinic phases. Conversely, at high temperatures around the nose, the nucleation rate becomes the limiting factor.

In Table 2, the temperature of the fastest transformation and the aging time at which 50% monoclinic content was reached in air, are reported for the present work in comparison to other Y-TZPs. It can be noticed that the temperature of the fastest transformation in the present work is lower than those reported for Y-TZP ceramics without alumina addition and the transformation is retarded compared to materials with comparable yttria content. This could be explained by the presence of alumina in the studied material. Indeed, it has been shown that the position of the C-curve for Y-TZPs in the TTT diagram depends on the grain size and the material's composition, in particular yttria and alumina contents [38,46-48]. Transformation curves shift towards higher temperature and shorted aging time by decreasing the yttria content [38,46-48]. On the other hand, increasing the alumina content retards the transformation [32] and consequently shifts the C-curve toward longer aging time [44].

The aging time at which 50% monoclinic content was reached for the present material (22 min) is significantly shorter than for 3Y-TZP without alumina (>150 min). This explains the high influence of the cooling rate on the phase transformation shown in Fig 4.

Table 2: Position of the transformation curves in the TTT diagram for the studied material in comparison with other Y-TZP materials. T_N is the temperature at the "nose" and t_{50} is the time at which the monoclinic content reached 50%.

Material composition		Position of the transformation curve		Reference
Y_2O_3 (% mol)	Al_2O_3 (% wt)	T_N (°C)	t_{50} (min)	
1	0	400	~0	[46]
1.5	0	427	8	[38]
	0	377	1	[47]
	0.25	**275**	**22**	**This work**
1.6	0	350	1	[45]
2	0	377	11	[46]
3	0	327	166	[38]
	1.2	250	~33*	[44]
	12	250	~208*	[44]

* In hours

Finally, the constructed TTT diagram provides evidence that relatively fast cooling is necessary to prevent t-m transformation after sintering or heat treatment of the studied 1.5Y-TZP. A cooling rate of at least 10°C/min is required to prevent transformation and thus the surface deterioration illustrated, as example in figure 12, for a sample cooled at 1°C/min after annealing at 600°C, for which the final volume fraction of the monoclinic phase was 90%, indicating an almost complete transformation of the surface. It is to note that only the first 5 microns below the surface are investigated by XRD in zirconia. Thus, having a 90 vol.% monoclinic content measured by XRD might not be detrimental for the bulk properties, but this remains a point of vigilance, especially for large parts that cannot be cooled down rapidly to avoid thermal shocks.

5. Conclusion

The studied material combines high mechanical properties and a high resistance to aging in water vapor at 134°C compared to the standard 3Y-TZP, which could be attributed to alumina addition and the relatively low sintering temperature.

Isothermal t-m phase transformation occurred in air at temperature ranged from 120 to 360°C and MAJ type kinetics was successfully applied, as for aging in water vapor between 100 and 140°C. The results indicated a strong dependence of the MAJ law exponent, n, on the temperature, with three separate stages, confirmed by optical observations. For temperatures below 180°C or above 340°C, n takes a low value (~ 0.6) which correspond to high nucleation rate. For a temperature range between 180°C and 340°C, the growth rate became dominant with high n value (between 3 and 4). It was shown that the nucleation stage at low temperatures is independent on the environment. Thus, the humidity in the air is sufficient to activate isothermal transformation.

A TTT diagram was constructed and it was shown that the transformation curves are shifted to lower temperature and to shorter aging time compared to standard 3Y-TZP without alumina addition. Therefore, a relatively high cooling rate, at least 10°C/min, is required to prevent the surface transformation after sintering or thermal treatments of the studied material.

References

[1] Evans, A. G., & Heuer, A. H. (1980). Transformation toughening in ceramics: Martensitic transformations in crack-tip stress fields. Journal of the American Ceramic Society, 63 (5-6), 241-248.

[2] Hannink, R. H., Kelly, P. M., & Muddle, B. C. (2000). Transformation toughening in zirconia-containing ceramics. Journal of the American Ceramic Society, 83 (3), 461-487.

[3] Chevalier, J., Gremillard, L., Virkar, A. V., & Clarke, D. R. (2009). The tetragonal-monoclinic transformation in zirconia: lessons learned and future trends. Journal of the american ceramic society, 92 (9), 1901-1920.

[4] Kobayashi, K., Kuwajima, H., & Masaki, T. (1981). Phase change and mechanical properties of ZrO2-Y2O3 solid electrolyte after ageing. Solid State Ionics, 3, 489-493.

[5] Lawson, S. (1995). Environmental degradation of zirconia ceramics. Journal of the European ceramic society, 15 (6), 485-502.

[6] Ban, S., Sato, H., Suehiro, Y., Nakanishi, H., & Nawa, M. (2008). Biaxial flexure strength and low temperature degradation of Ce-TZP/Al2O3 nanocomposite and Y-TZP as dental restoratives. Journal of Biomedical Materials Research Part B: Applied Biomaterials: An Official Journal of The Society for Biomaterials, The Japanese Society for Biomaterials, and The Australian Society for Biomaterials and the Korean Society for Biomaterials, 87 (2), 492-498

[7] Ramesh, S., Lee, K. S., & Tan, C. Y. (2018). A review on the hydrothermal ageing behaviour of Y-TZP ceramics. Ceramics International, 44 (17), 20620-20634.

[8] Matsui, K., Nakamura, K., Saito, M., Kuwabara, A., Yoshida, H., & Ikuhara, Y. (2022). Low-temperature degradation in yttria-stabilized tetragonal zirconia polycrystal: Effect of Y3+ distribution in grain interiors. Acta Materialia, 227, 117659.

[9] Deng, B., Zou, R., Huang, Y., Feng, L., & Chen, Y. (2023). Effect of grain boundary segregation on aging resistance and mechanical properties of tetravalent element-doped 3Y-TZP ceramics for dental restoration. International Journal of Smart and Nano Materials, 1-19.

[10] Chevalier, J. (2006). What future for zirconia as a biomaterial ?. Biomaterials, 27 (4), 535-543.

[11] Chevalier, J., Gremillard, L., & Deville, S. (2007). Low-temperature degradation of zirconia and implications for biomedical implants. Annual review of materials research, 37, 1-32.

[12] Roy, M. E., Whiteside, L. A., Katerberg, B. J., & Steiger, J. A. (2007). Phase transformation, roughness, and microhardness of artificially aged yttria-and magnesia-stabilized zirconia femoral heads. Journal of Biomedical Materials Research Part A: An Official Journal of The Society for Biomaterials, The Japanese Society for Biomaterials, and The Australian Society for Biomaterials and the Korean Society for Biomaterials, 83 (4), 1096-1102.

[13] Pereira, G. K. R., Venturini, A. B., Silvestri, T., Dapieve, K. S., Montagner, A. F., Soares, F. Z. M., & Valandro, L. F. (2016). Low-temperature degradation of Y-TZP ceramics: A systematic review and meta-analysis. Journal of the mechanical behavior of biomedical materials, 55, 151-163.

[14] Yang, H., & Ji, Y. (2016). Low-temperature degradation of zirconia-based all-ceramic crowns materials: a mini review and outlook. Journal of Materials Science & Technology, 32 (7), 593-596.

[15] Chevalier, J. (1997). Low temperature ageing behaviour of zirconia hip joint heads. Bioceramics, 10, 135-137.

[16] Yoshimura, M., Noma, T., Kawabata, K., & Sōmiya, S. (1989). Role of H2O on the degradation process of Y-TZP. Hydrothermal Reactions for Materials Science and Engineering: An Overview of Research in Japan, 396-398.

[17] Schubert, H., & Frey, F. (2005). Stability of Y-TZP during hydrothermal treatment: neutron experiments and stability considerations. Journal of the European Ceramic Society, 25 (9), 1597-1602.

[18] Schmauder, S., & Schubert, H. (1986). Significance of internal stresses for the martensitic transformation in Yttria-stabilized tetragonal zirconia polycrystals during degradation. Journal of the American Ceramic Society, 69 (7), 534-540.

[19] Gremillard, L., Chevalier, J., Epicier, T., Deville, S., & Fantozzi, G. (2004). Modeling the aging kinetics of zirconia ceramics. Journal of the European Ceramic Society, 24 (13), 3483-3489.

[20] Schneider, J., Begand, S., Kriegel, R., Kaps, C., Glien, W., & Oberbach, T. (2008). Low-temperature aging behavior of alumina-toughened zirconia. Journal of the American Ceramic Society, 91 (11), 3613-3618.

[21] Lucas, T. J., Lawson, N. C., Janowski, G. M., & Burgess, J. O. (2015). Phase transformation of dental zirconia following artificial aging. Journal of Biomedical Materials Research Part B: Applied Biomaterials, 103 (7), 1519-1523.

[22] Sato, T., & Shimada, M. (1985). Transformation of yttria-doped tetragonal ZrO2 polycrystals by annealing in water. Journal of the American Ceramic Society, 68 (6), 356-359.

[23] Lee, J. K., & Kim, H. (1994). Surface crack initiation in 2Y-TZP ceramics by low temperature aging. Ceramics international, 20 (6), 413-418.

[24] Lange, F. F. (1982). Transformation toughening: Part 3 Experimental observations in the ZrO2-Y2O3 system. Journal of Materials Science, 17, 240-246.

[25] Masaki, T. (1986). Mechanical properties of Y-PSZ after aging at low temperature. International Journal of High Technology Ceramics, 2 (2), 85-98.

[26] Li, J. F., & Watanabe, R. (1998). Phase transformation in Y2O3-partially-stabilized ZrO2 polycrystals of various grain sizes during low-temperature aging in water. Journal of the American Ceramic Society, 81 (10), 2687-2691.

[27] Munoz-Saldana, J., Balmori-Ramirez, H., Jaramillo-Vigueras, D., Iga, T., & Schneider, G. A. (2003). Mechanical properties and low-temperature aging of tetragonal zirconia polycrystals processed by hot isostatic pressing. Journal of materials research, 18 (10), 2415-2426.

[28] Hernandez, M. T., Jurado, J. R., Duran, P., & Fierro, J. L. (1991). Subeutectoid Degradation of Yttria-Stabilized Tetragonal Zirconia Polycrystal and Ceria-Doped Yttria-Stabilized Tetragonal Zirconia Polycrystal Ceramics. Journal of the American Ceramic Society, 74 (6), 1254-1258.

[29] Swab, J. J. (1991). Low temperature degradation of Y-TZP materials. Journal of Materials Science, 26, 6706-6714.

[30] Guo, X. (2004). Property degradation of tetragonal zirconia induced by low-temperature defect reaction with water molecules. Chemistry of materials, 16 (21), 3988-3994.

[31] Paul, A., Vaidhyanathan, B., & Binner, J. G. (2011). Hydrothermal aging behavior of nanocrystalline Y-TZP ceramics. Journal of the American Ceramic Society, 94 (7), 2146-2152.

[32] Zhang, F., Vanmeensel, K., Inokoshi, M., Batuk, M., Hadermann, J., Van Meerbeek, B., Naert I, Vleugels J. (2015). Critical influence of alumina content on the low temperature degradation of 2–3 mol% yttria-stabilized TZP for dental restorations. Journal of the European Ceramic Society, 35 (2), 741-750.

[33] Matsui, K., Yoshida, H., & Ikuhara, Y. (2014). Nanocrystalline, ultra-degradation-resistant zirconia: Its grain boundary nanostructure and nanochemistry. Scientific reports, 4 (1), 1-6.

[34] Gremillard, L., Chevalier, J., Epicier, T., & Fantozzi, G. (2002). Improving the durability of a biomedical-grade zirconia ceramic by the addition of silica. Journal of the American Ceramic Society, 85 (2), 401-407.

[35] Samodurova, A., Kocjan, A., Swain, M. V., & Kosmač, T. (2015). The combined effect of alumina and silica co-doping on the ageing resistance of 3Y-TZP bioceramics. Acta biomaterialia, 11, 477-487.

[36] Jansen, S. R., Winnubst, A. J. A., He, Y. J., Verweij, H., Van der Varst, P. T., & De With, G. (1998). Effects of grain size and ceria addition on ageing behaviour and tribological properties of Y-TZP ceramics. Journal of the European Ceramic Society, 18 (5), 557-563.

[37] Li, J. F., & Watanabe, R. (1997). Influence of a small amount of Al2O3 addition on the transformation of Y2O3-partially stabilized ZrO2 during annealing. Journal of materials science, 32, 1149-1153.

[38] Tsubakino, H. (2005). Isothermal tetragonal-to-monoclinic phase transformation in a zirconia–yttria system. Materials transactions, 46 (7), 1443-1451.

[39] Chevalier, J., Cales, B., & Drouin, J. M. (1999). Low-temperature aging of Y-TZP ceramics. Journal of the American Ceramic Society, 82 (8), 2150-2154.

[40] Li, J., Zhang, L., Shen, Q., & Hashida, T. (2001). Degradation of yttria stabilized zirconia at 370 K under a low applied stress. Materials Science and Engineering: A, 297 (1-2), 26-30.

[41] Lughi, V., & Clarke, D. R. (2007). Low-temperature transformation kinetics of electron-beam deposited 5 wt.% yttria-stabilized zirconia. Acta materialia, 55 (6), 2049-2055.

[42] Takigawa, Y., Shibano, T., Kanzawa, Y., & Higashi, K. (2009). Effect of small amount of insoluble dopant on tetragonal to monoclinic phase transformation in tetragonal zirconia polycrystal. Materials transactions, 50 (5), 1091-1095.

[43] Wei, C., & Gremillard, L. (2018). Towards the prediction of hydrothermal ageing of 3Y-TZP bioceramics from processing parameters. Acta Materialia, 144, 245-256.

[44] Tsubakino, H., Sonoda, K., & Nozato, R. (1993). Martensite transformation behaviour during isothermal ageing in partially stabilized zirconia with and without alumina addition. Journal of materials science letters, 12 (3), 196-198.

[45] Hayakawa, M., Nishio, K., Hamakita, J., & Onda, T. (1999). Isothermal and athermal martensitic transformations in a zirconia–yttria alloy. Materials Science and Engineering: A, 273, 213-217.

[46] Tsubakino, H., & Matsuura, N. (2002). Relationship between Transformation Temperature and Time-Temperature-Transformation Curves of Tetragonal-to-Monoclinic Martensitic Transformation in Zirconia-Yttria System. Journal of the American Ceramic Society, 85 (8), 2102-2106.

[47] Pee, J. H., Akao, T., Ohtsuka, S., & Hayakawa, M. (2003). The kinetics of isothermal martensitic transformation of zirconia containing a small amount of yttria. Materials transactions, 44 (9), 1783-1789.

[48] Pee, J. H., & Hayakawa, M. (2003). Isothermal martensitic transformation of zirconia doped with small amount of yttria. Journal de Physique IV (Proceedings), 112, 1107-1110.

[49] TOSOH, "Technical Data Sheet Zgaia™ 1.5Y-HT," Version 2.1, December 2021.

[50] Imariouane, M., Saâdaoui, M., Denis, G., Reveron, H., & Chevalier, J. (2023). Low-yttria doped zirconia: Bridging the gap between strong and tough ceramics. Journal of the European Ceramic Society, 43 (11), 4906-4915.

[51] Chevalier J, Liens A, Reveron H, Zhang F, Reynaud P, Douillard T, Preiss L, Sergo V, Lughi V, Swain M, Courtois N (2020). Forty years after the promise of «ceramic steel?»: Zirconia-based composites with a metal-like mechanical behavior. Journal of the American Ceramic Society, 103 (3), 1482-1513.

[52] Matsui, K., Hosoi, K., Feng, B., Yoshida, H., & Ikuhara, Y. (2023). Ultrahigh toughness zirconia ceramics. Proceedings of the National Academy of Sciences, 120 (27), e2304498120.

[53] Yamashita, I., Tsukuma, K., Tojo, T., Kawaji, H., & Atake, T. (2008). Synchrotron X-ray study of the crystal structure and hydrothermal degradation of yttria-stabilized tetragonal zirconia polycrystal. Journal of the American Ceramic Society, 91 (5), 1634-1639.

[54] Kern, F., & Gadow, R. (2013). Mechanical properties and low temperature degradation resistance of 2.5 Y-TZP–alumina composites. Materiały Ceramiczne, 65 (3), 258-266.

[55] Kern, F., Kabir, A., & Gadow, R. (2017). Mechanical properties and low temperature degradation resistance of alumina-doped 3Y-TZP fabricated from stabilizer coated powders. Ceramic Materials, 69, 279-285.

[56] Kern, F., Lindner, V., & Gadow, R. (2016). Low-temperature degradation behaviour and mechanical properties of a 3Y-TZP manufactured from detonation-synthesized powder. Journal of Ceramic Science and Technology, 7 (04), 313-322.

[57] Cattani-Lorente, M., Durual, S., Amez-Droz, M., Wiskott, H. A., & Scherrer, S. S. (2016). Hydrothermal degradation of a 3Y-TZP translucent dental ceramic: A comparison of numerical predictions with experimental data after 2 years of aging. Dental Materials, 32 (3), 394-402.

[58] Jing, Q., Bao, J., Ruan, F., Song, X., An, S., Zhang, Y., Tian, Z., Xie, M., & Gao, J. (2019). The effect of YF3 on the mechanical properties and low-temperature degradation of 3Y-TZP ceramics. Ceramics International, 45 (18), 24212-24220.

[59] Belli, R., Loher, C., Petschelt, A., Cicconi, M. R., de Ligny, D., Anglada, M., & Lohbauer, U. (2020). Low-temperature degradation increases the cyclic fatigue resistance of 3Y-TZP in bending. Dental Materials, 36 (8), 1086-1095.

[60] Cattani-Lorente, M., Scherrer, S. S., Durual, S., Sanon, C., Douillard, T., Gremillard, L., Chevalier, J., & Wiskott, A. (2014). Effect of different surface treatments on the hydrothermal degradation of a 3Y-TZP ceramic for dental implants. Dental Materials, 30 (10), 1136-1146.

[61] Chevalier, J., Loh, J., Gremillard, L., Meille, S., & Adolfson, E. (2011). Low-temperature degradation in zirconia with a porous surface. Acta biomaterialia, 7 (7), 2986-2993.

[62] Yamashita, I., & Tsukuma, K. (2005). Phase separation and hydrothermal degradation of 3 mol% Y2O3-ZrO2 ceramics. Journal of the Ceramic Society of Japan, 113 (1320), 530-533.

[63] Zhang, F., Inokoshi, M., Batuk, M., Hadermann, J., Naert, I., Van Meerbeek, B., & Vleugels, J. (2016). Strength, toughness and aging stability of highly-translucent Y-TZP ceramics for dental restorations. Dental Materials, 32 (12), 327-337.

[64] Xie, Q. F., Wang, C., Zan, Q. F., & Dong, L. M. (2010). Apparent Activation Energy in Low Temperature Aging of Y-TZP Ceramics. Advanced Materials Research, 105, 100-103.

[65] Kohorst, P., Borchers, L., Strempel, J., Stiesch, M., Hassel, T., Bach, F. W., & Hübsch, C. (2012). Low-temperature degradation of different zirconia ceramics for dental applications. Acta Biomaterialia, 8 (3), 1213-1220.

[66] Cattani-Lorente, M., Scherrer, S. S., Ammann, P., Jobin, M., & Wiskott, H. A. (2011). Low temperature degradation of a Y-TZP dental ceramic. Acta biomaterialia, 7 (2), 858-865.

[67] Elshazly, E. S., Ali, M. E. S., & El-Hout, S. M. (2008). Alumina effect on the phase transformation of 3Y-TZP ceramics. Journal of materials science & technology, 24 (6), 873.

[68] Inokoshi, M., Zhang, F., De Munck, J., Minakuchi, S., Naert, I., Vleugels, J., Van Meerbeek, B., & Vanmeensel, K. (2014). Influence of sintering conditions on low-temperature degradation of dental zirconia. Dental materials, 30 (6), 669-678.

[69] Kim, D. J., Jung, H. J., & Cho, D. H. (1995). Phase transformations of Y2O3 and Nb2O5 doped tetragonal zirconia during low temperature aging in air. Solid State Ionics, 80 (1-2), 67-73.

[70] Kim, D. J. (1997). Influence of aging environment on low-temperature degradation of tetragonal zirconia alloys. Journal of the European Ceramic Society, 17 (7), 897-903.

[71] Tsubakino, H., Nozato, R., & Hamamoto, M. (1991). Effect of alumina addition on the tetragonal-to-monoclinic phase transformation in zirconia–3 mol% yttria. Journal of the American Ceramic Society, 74 (2), 440-443.

[72] Garvie, R. C., & Nicholson, P. S. (1972). Phase analysis in zirconia systems. Journal of the American Ceramic Society, 55 (6), 303-305.

[73] Toraya, H., Yoshimura, M., & Somiya, S. (1984). Calibration curve for quantitative analysis of the monoclinic-tetragonal ZrO2 system by X-ray diffraction. Journal of the American Ceramic Society, 67 (6), C-119.

[74] Stevens, R. (1986). An introduction to zirconia: zirconia and zirconia ceramics 2nd ed. Magnesium Elektron Ltd, Twickenham.

[75] Matsui, K., Yamakawa, T., Uehara, M., Enomoto, N., & Hojo, J. (2008). Mechanism of alumina-enhanced sintering of fine zirconia powder: influence of alumina concentration on the initial stage sintering. Journal of the American Ceramic Society, 91 (6), 1888-1897.

[76] Bučevac, D., Kosmač, T., & Kocjan, A. (2017). The influence of yttrium-segregation-dependent phase partitioning and residual stresses on the aging and fracture behaviour of 3Y-TZP ceramics. Acta biomaterialia, 62, 306-316.

[77] Zhang, B., Isobe, T., Satani, S., & Tsubakino, H. (1999). The effect of alumina addition on phase transformation and mechanical properties in partially stabilized zirconia. Key Engineering Materials, 161.

Tables captions:

Table 1: MAJ parameter, *n*, and activation energy, *Q*, for Y-TZP ceramics aged in air or in water vapor. T_A is the temperature of aging.

Table 2: Position of the transformation curves in the TTT diagram for the studied material in comparison with other Y-TZP materials. T_N is the temperature at the "nose" and t_{50} is the time at which the monoclinic content reached 50%.

Figures captions:

Figure 1: Variation of the monoclinic phase content versus time during hydrothermal aging between 100 and 140°C.

Figure 2: Example of in-situ XRD pattern during isothermal transformation in air at 250°C.

Figure 3: Variation of the monoclinic phase content versus time in air between 120 and 360°C.

Figure 4: Effect of the cooling rate on tetragonal to monoclinic phase transformation. Samples were previously annealed at 600°C during 20 min. The arrow indicates the direction of temperature variation.

Figure 5: Reverse monoclinic to tetragonal phase transformation during heating. The arrow indicates the direction of temperature variation.

Figure 6: Mehl–Avrami–Johnson plot of the experimental data of figure 1, corresponding to hydrothermal aging at various temperatures. For each temperature, the obtained value of the exponent n is indicated in brackets. The unit of time is seconds.

Figure 7: Mehl–Avrami–Johnson plot of the experimental data of Figure 3, corresponding to aging at various temperatures in air between 120 and 350°C. For each temperature, the obtained value of the exponent n is indicated in brackets. The unit of time is seconds.

Figure 8: Variation of the exponent n of MAJ law (eq. (1)) with temperature. Open symbols correspond to hydrothermal aging in autoclave and solid symbols to aging in air.

Figure 9: Representative examples of optical micrographs with Nomarski contrast showing the surface of samples aged in air at temperatures of 134, 250, 275 and 360°C, with a final monoclinic content respectively of 65%, 85%, 85% and 77%. The arrows indicate examples of nucleation sites.

Figure 10: ln *b* versus 1/*T* (eq. (2)) for aging in water vapor and air.

Figure 11: Time-Temperature-Transformation (TTT) curves derived from the results of the isothermal transformations curves of Fig. 3. The dashed line indicates an approximate position of the start temperature for the t-m transformation, M_s.

Figure 12: Optical micrograph of a sample cooled at a slow rate of 1°C/min after annealing at 600°C. The final volume fraction of the monoclinic phase measured at the surface was of 90%.

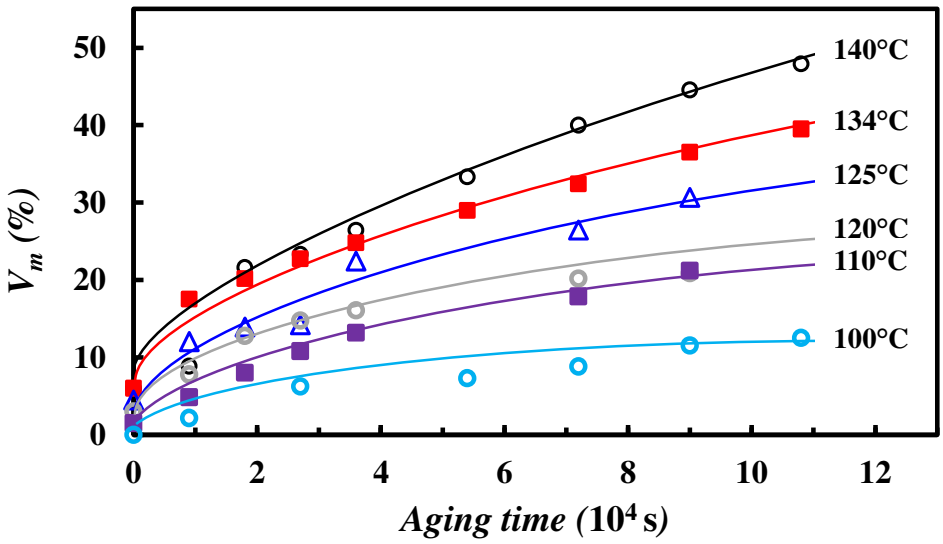

Figure 1: Variation of the monoclinic phase content versus time during hydrothermal aging between 100 and 140°C.

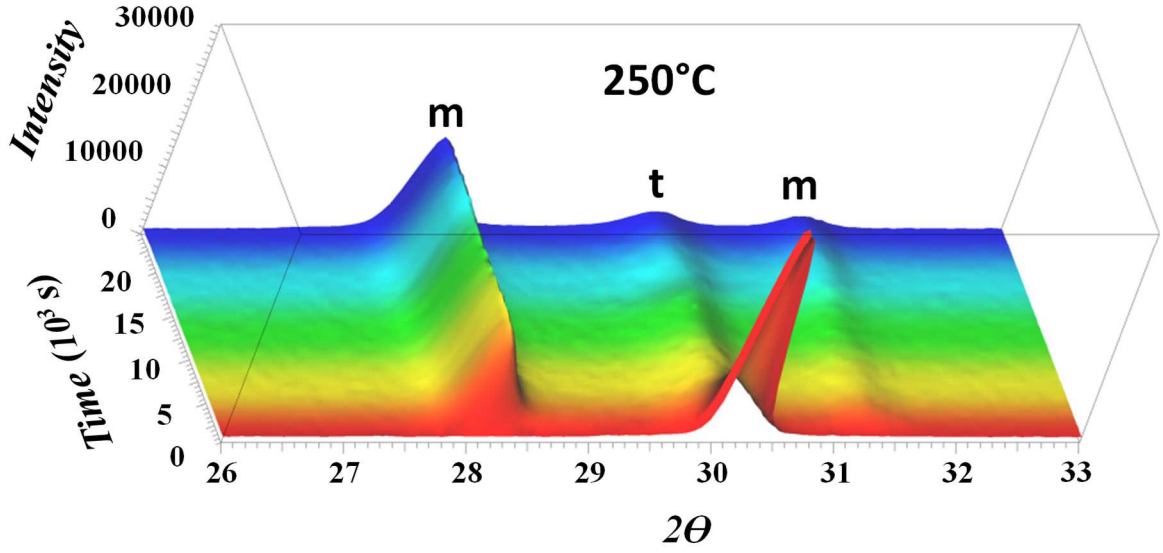

Figure 2: Example of in-situ XRD pattern during isothermal transformation in air at 250°C.

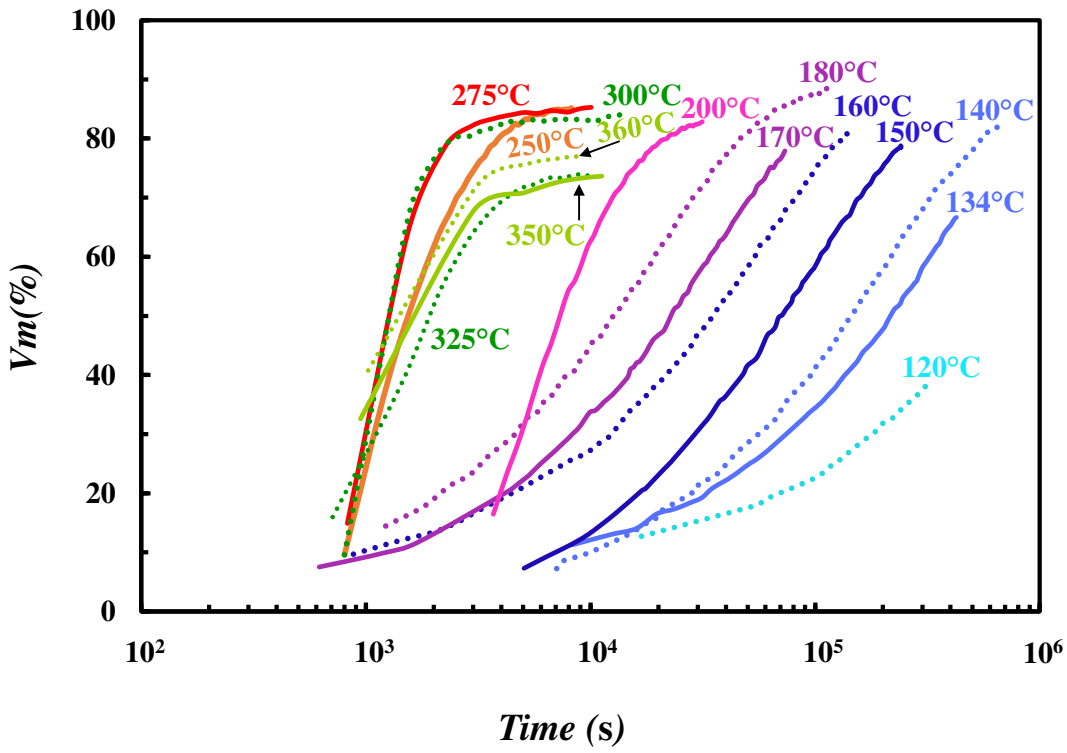

Figure 3: Variation of the monoclinic phase content versus time in air between 120 and 360°C.

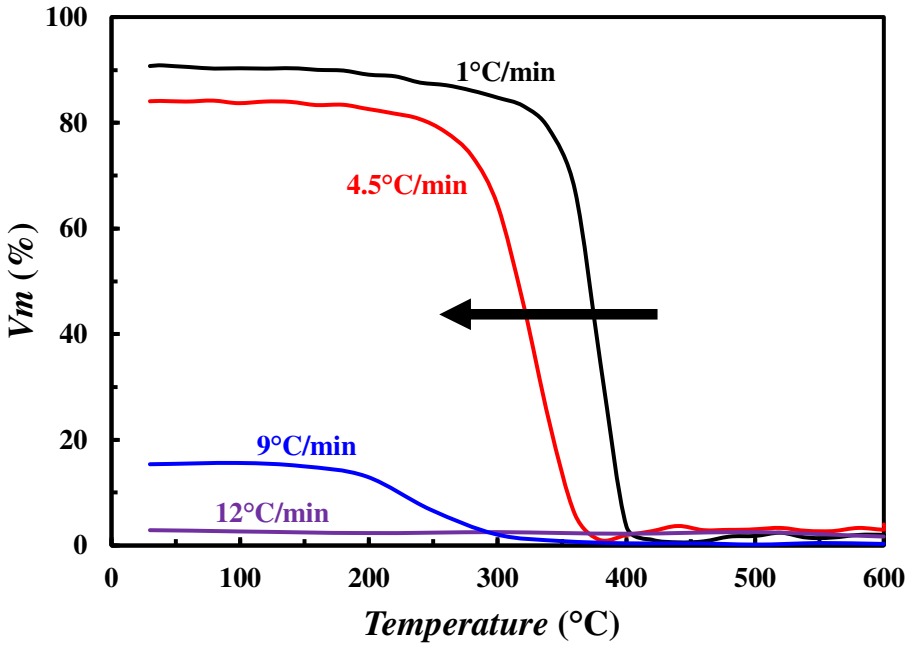

Figure 4: Effect of the cooling rate on tetragonal to monoclinic phase transformation. Samples were previously annealed at 600°C during 20 min. The arrow indicates the direction of temperature variation.

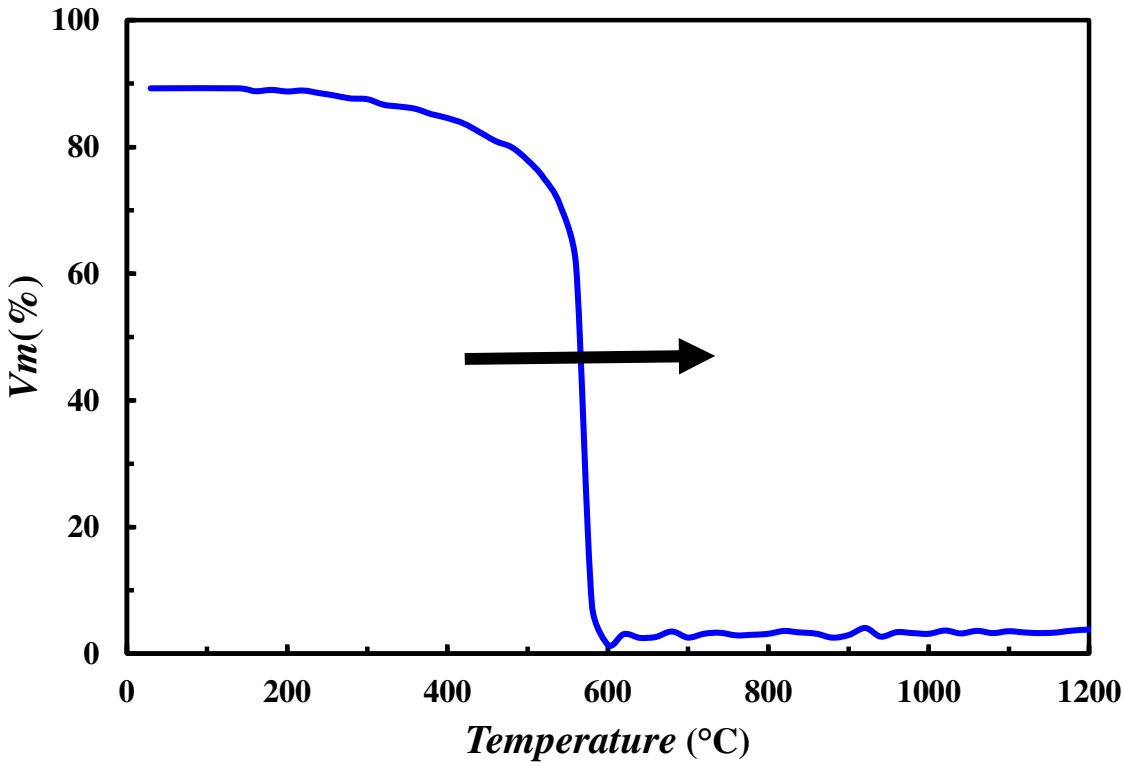

Figure 5: Reverse monoclinic to tetragonal phase transformation during heating. The arrow indicates the direction of temperature variation.

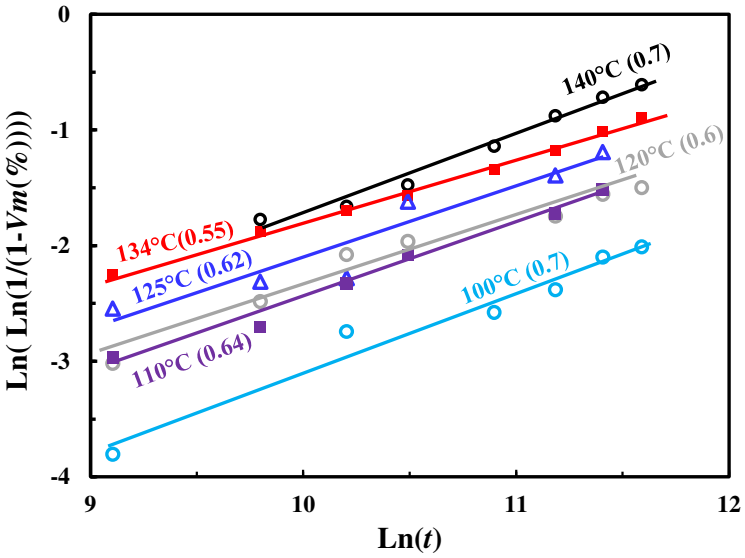

Figure 6: Mehl–Avrami–Johnson plot of the experimental data of figure 1, corresponding to hydrothermal aging at various temperatures. For each temperature, the obtained value of the exponent n is indicated in brackets. The unit of time is seconds.

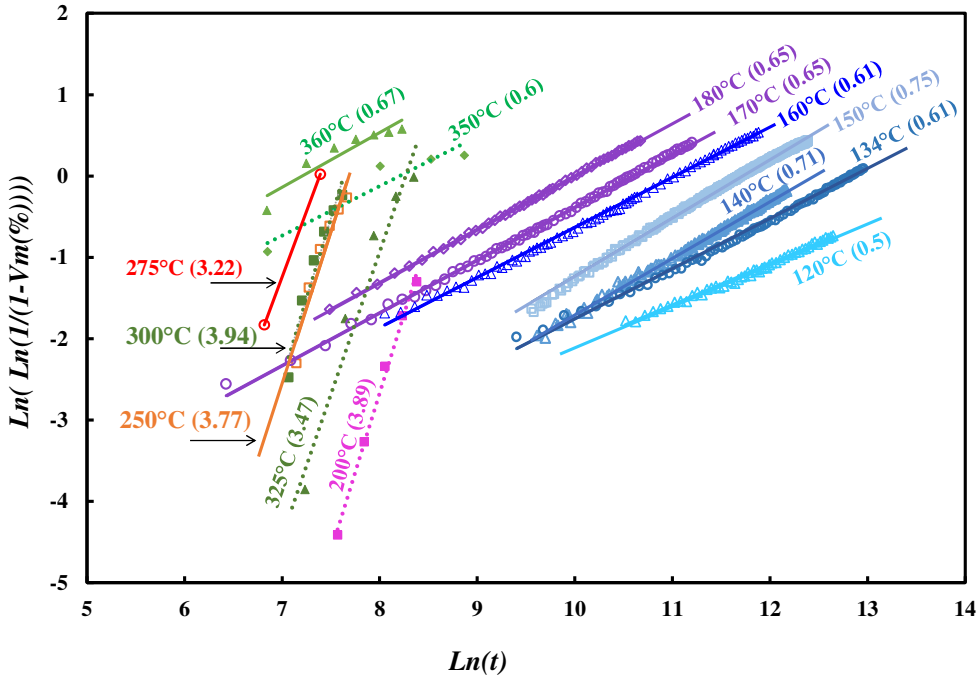

Figure 7: Mehl–Avrami–Johnson plot of the experimental data of Figure 3, corresponding to aging at various temperatures in air between 120 and 350°C. For each temperature, the obtained value of the exponent n is indicated in brackets. The unit of time is seconds.

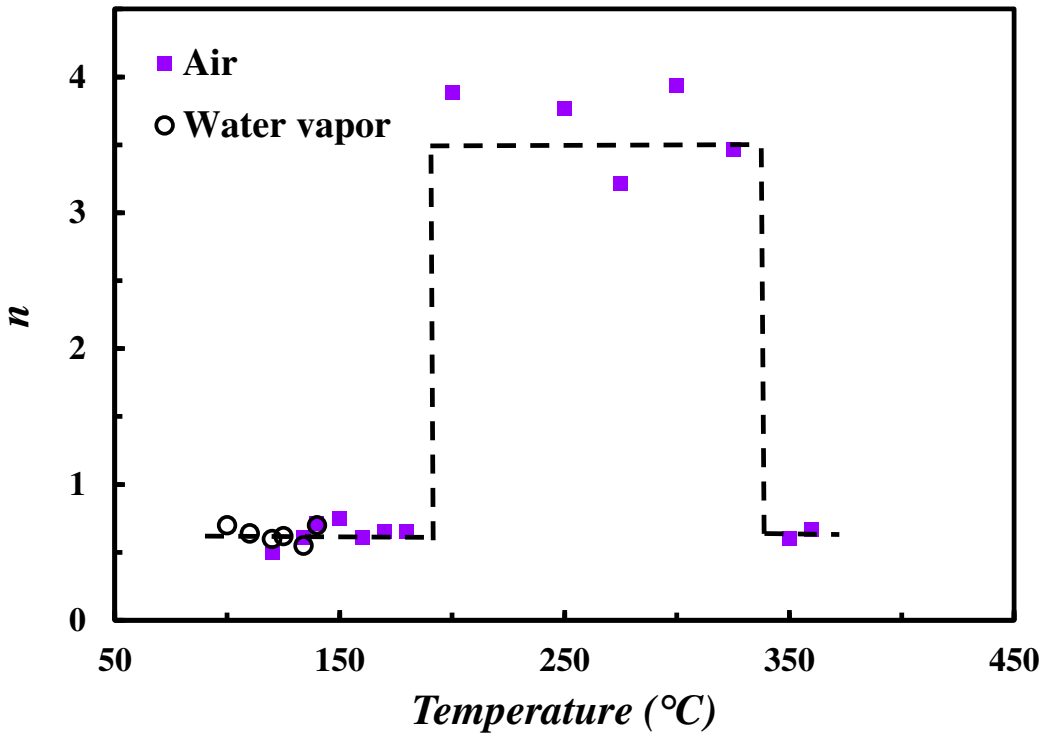

Figure 8: Variation of the exponent n of MAJ law (eq. (1)) with temperature. Open symbols correspond to hydrothermal aging in autoclave and solid symbols to aging in air.

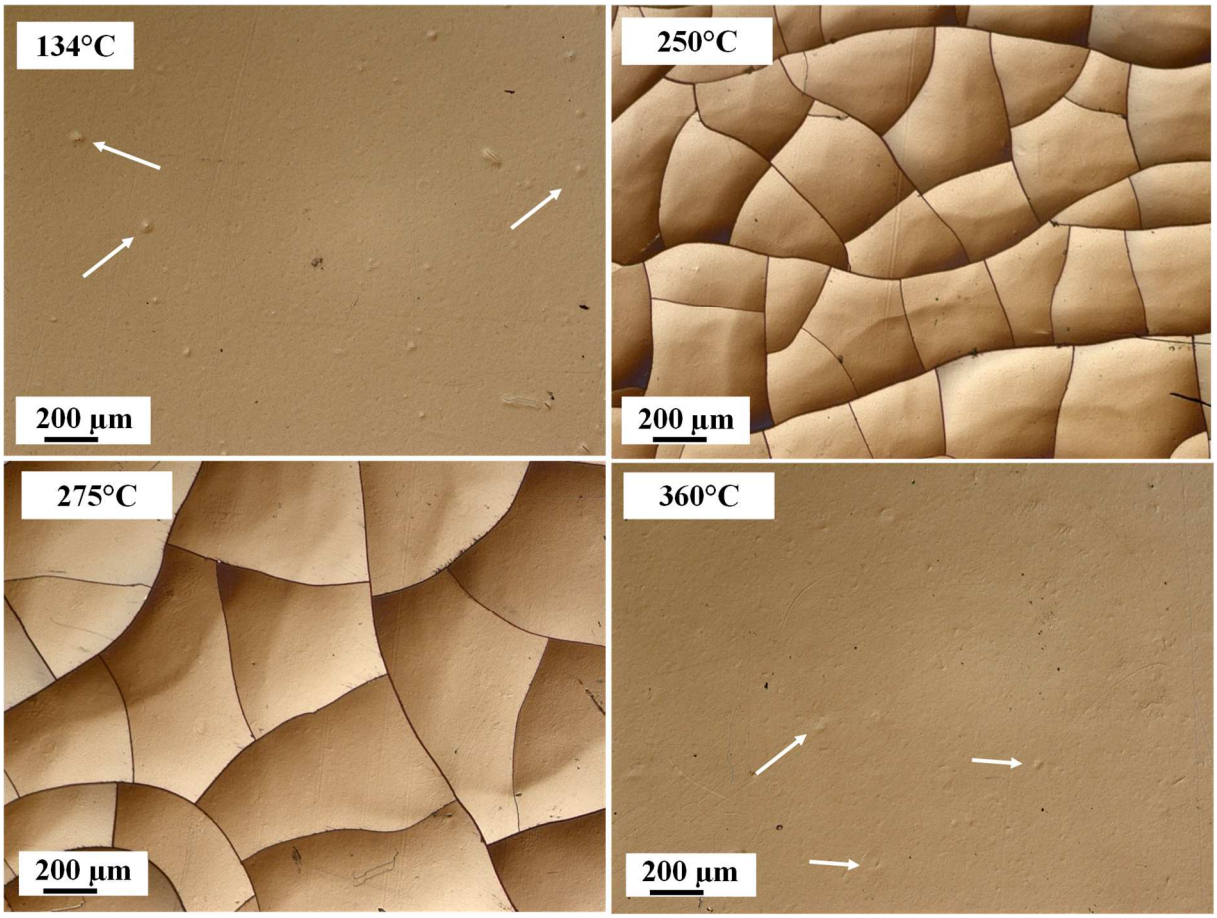

Figure 9: Representative examples of optical micrographs with Nomarski contrast showing the surface of samples aged in air at temperatures of 134, 250, 275 and 360°C, with a final monoclinic content respectively of 65%, 85%, 85% and 77%. The arrows indicate examples of nucleation sites.

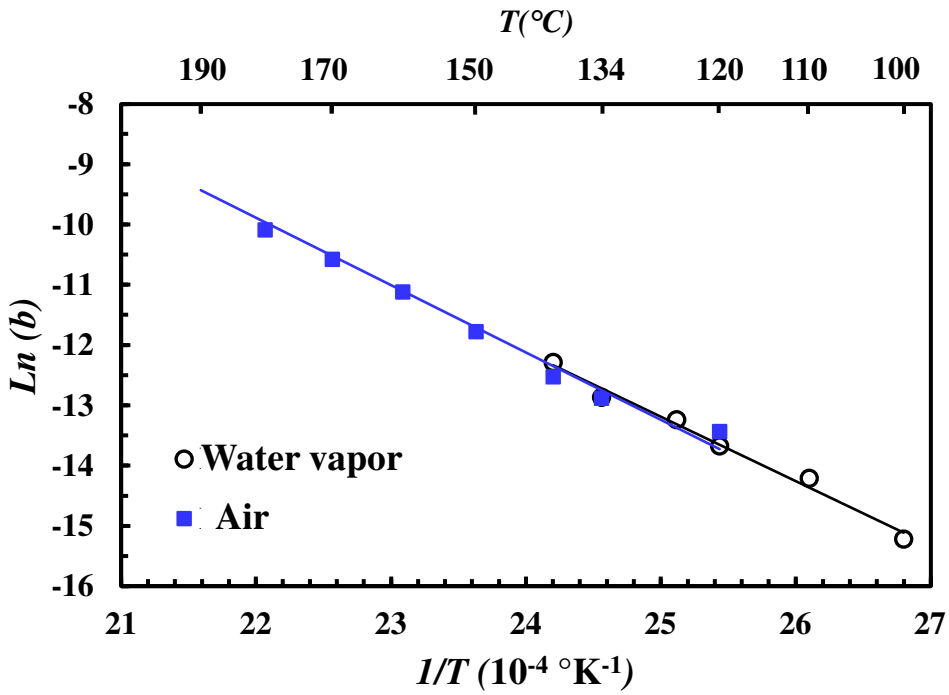

Figure 10: ln *b* versus 1/*T* (eq. (2)) for aging in water vapor and air.

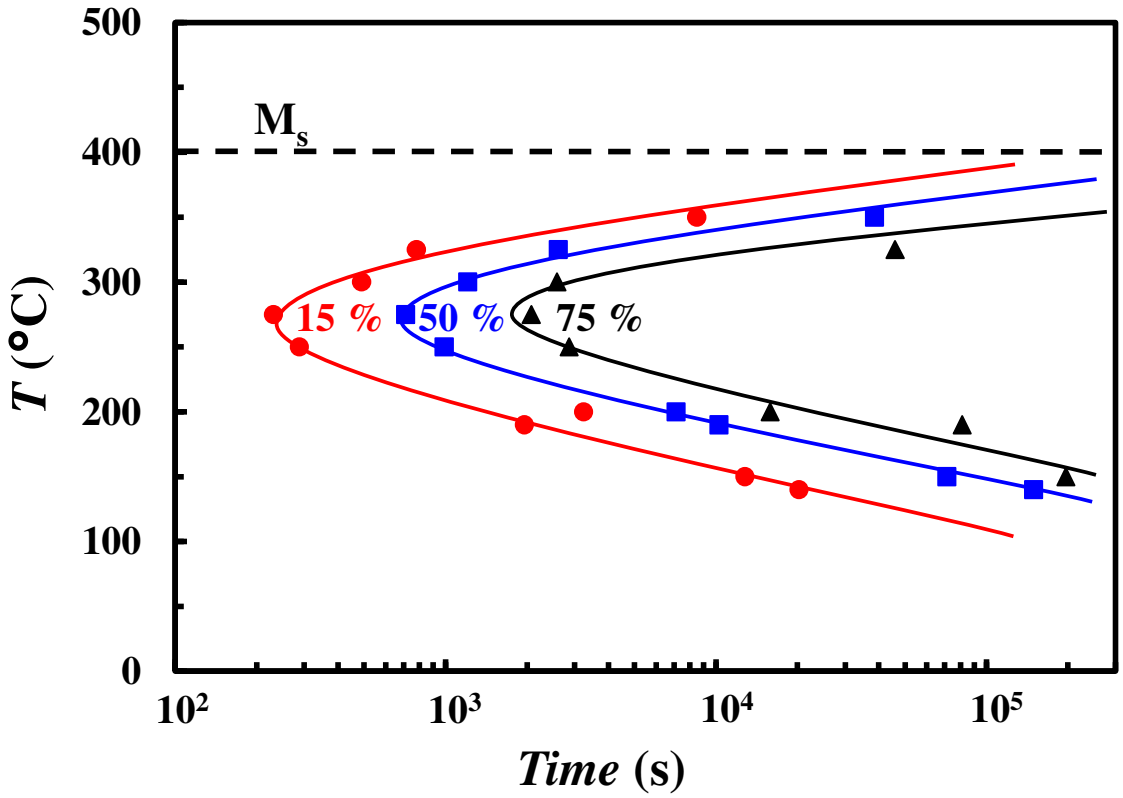

Figure 11: Time-Temperature-Transformation (TTT) curves derived from the results of the isothermal transformations curves of Fig. 3. The dashed line indicates an approximate position of the start temperature for the t-m transformation, M_s.

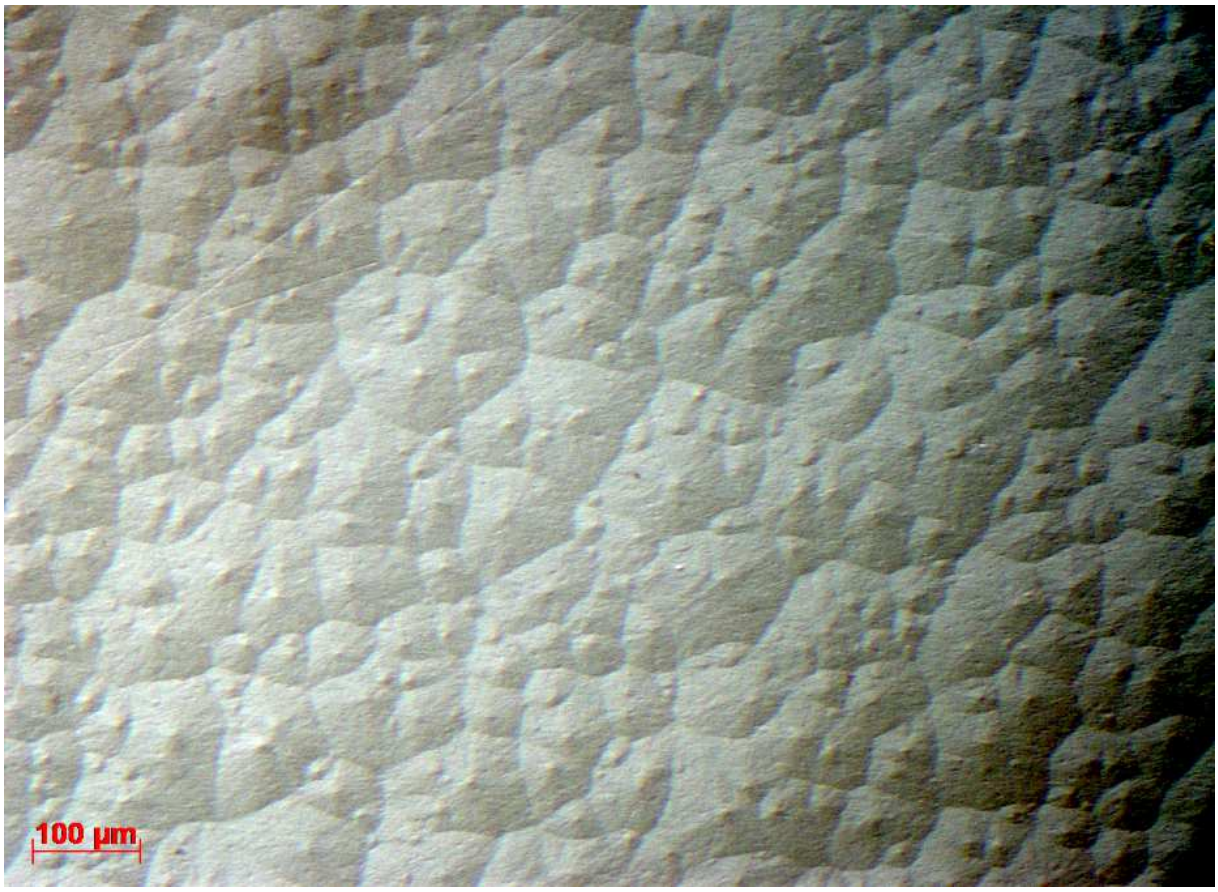

Figure 12: Optical micrograph of a sample cooled at a slow rate of 1°C/min after annealing at 600°C. The final volume fraction of the monoclinic phase measured at the surface was of 90%.